J Biomol NMR (2011) 50:19–33
DOI 10.1007/s10858-011-9474-8

ARTICLE

Density functional calculations of backbone ^{15}N shielding tensors in beta-sheet and turn residues of protein G

Ling Cai · Daniel S. Kosov · David Fushman

Received: 21 October 2010 / Accepted: 18 January 2011 / Published online: 9 February 2011

Abstract We performed density functional calculations of backbone ^{15}N shielding tensors in the regions of beta-sheet and turns of protein G. The calculations were carried out for all twenty-four beta-sheet residues and eight beta-turn residues in the protein GB3 and the results were compared with the available experimental data from solid-state and solution NMR measurements. Together with the alpha-helix data, our calculations cover 39 out of the 55 residues (or 71%) in GB3. The applicability of several computational models developed previously (Cai et al. in J Biomol NMR 45:245–253, 2009) to compute ^{15}N shielding tensors of alpha-helical residues is assessed. We show that the proposed quantum chemical computational model is capable of predicting isotropic ^{15}N chemical shifts for an entire protein that are in good correlation with experimental data. However, the individual components of the predicted ^{15}N shielding tensor agree with experiment less well: the computed values show much larger spread than the experimental data, and there is a profound difference in the behavior of the tensor components for alpha-helix/turns and beta-sheet residues. We discuss possible reasons for this.

Keywords Nitrogen-15 shielding tensor · Ab initio calculation · Density-functional calculation · Beta-sheet · Turns · Protein G

Introduction

Chemical shifts reflect the local electronic environment of a nucleus and are the primary NMR characteristics distinguishing various nuclei in a molecule. Chemical shift measurements in proteins play an increasingly important role in characterization of protein secondary and tertiary structure (Wishart et al. 1992; Cornilescu et al. 1999; Lipsitz and Tjandra 2003; Shen and Bax 2007; Shen et al. 2008; Shen et al. 2009a; Shen et al. 2009b; Shen et al. 2009c; Wylie et al. 2009) and dynamics (Fushman and Cowburn 2001; Hall and Fushman 2006), protein folding pathways (Sadqi et al. 2006), protein structure validation (Spronk et al. 2004), as well as in mapping out interaction interfaces (Varadan et al. 2002; Zuiderweg 2002) and quantification of the strength of protein–ligand binding (Varadan et al. 2004; Varadan et al. 2005; Zhang et al. 2009). The anisotropic character of the shielding tensors can also be utilized to study membrane proteins and other oriented systems by means of solid-state NMR spectroscopy (reviewed in (Saito et al. 2010)). The ability to make an accurate prediction of chemical shifts from first principles and directly from the structure is critical for success of these NMR approaches, especially the emerging methods for predicting protein 3D structures directly from chemical shifts (Shen et al. 2008; Shen et al. 2009a).

Electronic supplementary material The online version of this article (doi:10.1007/s10858-011-9474-8) contains supplementary material, which is available to authorized users.

L. Cai · D. S. Kosov · D. Fushman
Department of Chemistry and Biochemistry,
University of Maryland, College Park, MD 20742, USA

L. Cai · D. Fushman (✉)
Center for Biomolecular Structure and Organization,
University of Maryland, 1115 Biomolecular Sciences Bldg
(#296), College Park, MD 20742-3360, USA
e-mail: fushman@umd.edu

D. S. Kosov (✉)
Department of Physics and Center for Nonlinear Phenomena
and Complex Systems, Université Libre de Bruxelles, Campus
Plaine, CP 231, Blvd du Triomphe, 1050 Brussels, Belgium
e-mail: dkosov@ulb.ac.be

Various theoretical methods and computational schemes have been developed in the past decades for chemical shift calculations in peptides and proteins (reviewed in (Shen and Bax 2007)). They range from ab initio quantum chemical calculations (de Dios et al. 1993; Oldfield 1995; Xu and Case 2001; Xu and Case 2002) to those based on sequence homology (Wishart et al. 1997; Shen and Bax 2007) or empirical shielding surface (Neal et al. 2003). While the knowledge-based, empirical methods (e.g., SHIFTX Neal et al. 2003, SPARTA Shen and Bax 2007 etc.) are fast and have significantly improved the accuracy of isotropic chemical shifts predictions in proteins, first principles calculations directly from the three-dimensional structure require significant computational efforts and thus have been mostly limited to relatively small molecular fragments. However, ab initio quantum mechanical calculations provide a unique opportunity not only to fully characterize the shielding tensors, but—perhaps most importantly—to elucidate contributions from various factors (structure, charges, interactions, conformational dynamics, solvent effects etc.) that determine and control chemical shielding in proteins. Therefore, the utility of ab initio approaches as a means of gaining detailed understanding of the nature of shielding tensors and their relationship with protein structure cannot be overestimated.

Of all nuclei in a protein molecule, backbone ^{15}N presents the biggest challenge because ^{15}N chemical shifts are influenced by numerous factors none of which appears dominant: the identity of the current and preceding amino acids, backbone and side chain torsion angles (ϕ, ψ, χ_1), hydrogen bonding and direct interactions with nearby side chains, long-range intra-protein electrostatics, and solvent effect (de Dios et al. 1993; Le and Oldfield 1996; Brender et al. 2001; Xu and Case 2002; Poon et al. 2004; Cai et al. 2009). In addition, the calculations must take into account the dynamic nature of the protein structural ensemble and possible charge fluctuations of the ionizable groups, in order to provide a more realistic picture of a protein and account for chemical shift's sensitivity to experimental conditions (pH, temperature, etc.; see e.g. Vila and Scheraga 2008). On the other hand, due to the relatively low cost of ^{15}N-enrichment and high sensitivity of ^{15}N shielding to local electronic environment, ^{15}N is widely used as a sensitive reporter group for protein NMR studies. The applications include protein dynamics studies (taking advantage of ^{15}N–^{1}H being an isolated spin-pair), protein fingerprinting (^{15}N–^{1}H maps), and interface mapping and quantification of the strength of protein–ligand interactions (Zuiderweg 2002; Varadan et al. 2004; Varadan et al. 2005; Zhang et al. 2008; Zhang et al. 2009). ^{15}N chemical shift tensors in short model peptides have been extensively studied by solid state NMR spectroscopy (see e.g. Oas et al. 1987; Hiyama et al. 1988; Ramamoorthy et al. 1995; Lee and Ramamoorthy 1998; Lee et al. 2001; Saito et al. 2010).

Recently, we developed and applied a computational model that includes most of the important effects in density functional calculations of backbone ^{15}N shielding tensors for selected residues in the α-helix of the B3 domain of streptococcal protein G (GB3; Cai et al. 2009). Our results were in good agreement with experimental NMR data. Compared to a regular α-helix, where the backbone torsion angles are relatively fixed and each residue (except for the first and last turns) has two hydrogen bonding (HB) partners, other secondary structure elements (β-strands, turns/loops) have a greater variability in both the torsion angles and the number of HB partners, and therefore are presumably more difficult to model. Here we present follow-up calculations of backbone ^{15}N shielding tensors for all 24 β-sheet residues and eight turn residues in the same protein and compare our results with available experimental data from solid-state and solution NMR measurements. Together with the α-helix data, our calculations cover 39 out of the 55 (or 71%) residues in GB3. We show that current density functional methods are capable of predicting ^{15}N chemical shifts in an entire protein that are in good correlation with experimental data. We also found that the individual components of the calculated ^{15}N shielding tensor agree with experiment less well, namely, the computed values show a much larger spread than the experimental data, and there is a marked difference in the behavior of the tensor components for α-helix/turns and β-sheet residues.

Computational methods

All calculations were performed using the GAUSSIAN03 suite of programs (Frisch et al. 2004). We used density-functional theory (DFT) utilizing three-parameter Becke-Lee–Yang–Parr (B3LYP) exchange–correlation functional (Becke 1988; Lee et al. 1988; Becke 1993). The assignments of the basis sets were the same as in our earlier paper (Cai et al. 2009). Specifically, for the residue of interest i we applied a $6-311+G(2d,p)$ basis set for the four atoms in the peptide plane to which N_i belongs, as well as the $C\alpha_i$. Where applicable, the direct and indirect HB partners provide a carbonyl oxygen and an amide nitrogen, respectively, as the acceptor and the donor of the hydrogen bond. The peptide planes the two hydrogen-bonded atoms belong to, as well as the Cα atoms directly bonded with the corresponding C′ or N atoms were also assigned the $6-311+G(2d,p)$ basis set. For the remaining atoms in the model a 4–21G basis set was applied.

The charged field perturbation (CFP) calculations were performed using the same atomic charge set (AMBER

(Cornell et al. 1995)) as in the previous calculations for α-helical residues (Cai et al. 2009). The atom coordinates were taken from the best representative conformer of GB3 structure (PDB code: 2OED), obtained by refinement of the crystal structure by backbone residual dipolar couplings (RDC; Ulmer et al. 2003), without further geometry optimization.

To calculate the ^{15}N chemical shielding of residue i in the β-sheet, we included a main fragment consisting of residues i and $i-1$. The hydrogen-bonding (HB) partners, both direct and indirect (if applicable), were included as additional fragments. This resulted in either a "two-fragment" or a "three-fragment" model for β-sheet residues depending on the number of HB partners (referred to as the *fragment* models; Fig. 1c). The end-groups of the main fragment and the HB partners were modified in the same way as in our previous calculations for α-helical residues (Cai et al. 2009). Namely, the main fragment had the N-terminus capped by a formyl group (–COH) and the C-terminus capped by an amino group (–NH_2), and the hydrogen bonding partners were modified to be CH_3–CO–(NH–CH(R)–CO)–NH–CH_3 where (R) is the corresponding side chain. The basis set assignments were performed as specified above (see also Fig. 1c).

In light of the previous literature (Xu and Case 2002; Villegas et al. 2007), we also carried out calculations using a more complex, *extended* model which included the entire β-strand carrying residue i as well as its immediate neighboring β-strand(s) (also as entire strand(s)) (Fig. 1d). Specifically, for residues in strands β2 or β3 the calculations included a two-strand fragment (β2–β1 or β3–β4, respectively), while three-strand fragments (β2–β1–β4 or β1–β4–β3) were used in the calculations for β1 or β4, respectively. In this model, except for the residues i and $i-1$ and the hydrogen bonding partners of residue i, all non-glycine and non-alanine residues were modified to be alanines. As the extended model builds upon the fragment model, the same atoms as in the fragment model were assigned the 6 − 311 + G(2d,p) basis set, while the rest of the atoms were assigned the less dense 4–21G basis set (see Fig. 1d).

Calculations of ^{15}N shieldings in the β-turns were performed in a similar way, except that only the main fragment (of varying length) was included and contained at least the entire turn (4-residues).

Results

We performed density functional calculations of ^{15}N shielding tensors for all 24 β-sheet residues in GB3. This protein has been extensively studied by various NMR techniques (Hall and Fushman 2003; Ulmer et al. 2003; Hall and Fushman 2006; Vasos et al. 2006; Nadaud et al. 2007), and its crystal structure is available at 1.1 Å resolution (Derrick and Wigley 1994). The β-sheet residues can be sorted into three groups according to the number and nature of HB partners they have (see Fig. 1 and Table 1). Various residue fragment models were used in our calculations depending on the HB pattern, see "Computational methods". We also performed similar calculations for all eight residues in the turns (β1/β2 and β3/β4) connecting these β-strands.

^{15}N Shielding tensor elements

The calculated ^{15}N shielding tensors ($\underline{\underline{\sigma}}$) for β-sheet residues are presented in Supplementary Table S1. As expected, the intermediate component (σ_{22}) of the tensor is almost orthogonal to the peptide plane, while the other two components lie close to the peptide plane. The least-shielded component (σ_{11}) is slightly tilted out of the peptide plane (tilt angle from −6° to 4°) and makes an angle of 12.5°–24.8° with the NH bond. The anisotropies (CSA = $\sigma_{11} - (\sigma_{22} + \sigma_{33})/2$) of the calculated shielding tensors range from −132.8 ppm to −185.6 ppm, and their rhombicities ($\eta = (\sigma_{22} - \sigma_{33})/(\sigma_{11} - \sigma_{iso})$, where $\sigma_{iso} = \mathrm{tr}\{\underline{\underline{\sigma}}\}/3$) range from 0.17 to 0.62.

We first compared the individual components of the shielding tensors with available data for experimental chemical shift tensors for protein GB1 measured using slow magic angle spinning solid-state NMR (Wylie et al. 2007). GB1 and GB3, the first and third, respectively, immunoglobulin-binding domains of the streptococcal protein G, are highly homologous. Their amino acid sequences differ by only four residues in the β-sheet (6, 7, 19, and 42) and two in the α-helix (24, 29), while the (backbone) three-dimensional structures are almost identical: the crystal structures of GB3 (PDB code: 1IGD(Derrick and Wigley 1994)) and GB1 (PDB code: 2PGA(Gallagher et al. 1994)) superimpose with a backbone RMSD of 0.27 Å. The individual principal components of the calculated ^{15}N shielding tensor for the β-sheet residues in GB3 are in overall good agreement with the experimental data for GB1 (Fig. 2). The corelation coefficient is $r = -0.98$; the regression line has a slope close to an ideal of −1 and an intercept of 241.43 ± 4.32 ppm, comparable to those for α-helical residues (Cai et al. 2009). Combining both β-sheet and α-helix residues gives similar results (Fig. 2): $r = -0.99$, slope = −1.01 ± 0.02, and intercept = 243.94 ± 3.29 ppm. Note that because the slope is −1, the intercept of the regression line in Fig. 2 has the meaning of the reference shielding. It is therefore noteworthy that its value obtained here agrees nicely with the absolute ^{15}N shielding (244.6 ppm) of liquid ammonia at ambient temperature (Jameson et al. 1981), on which the ^{15}N chemical shift referencing is based (Wishart et al. 1995; Markley et al. 1998; Harris et al. 2008). This shows that

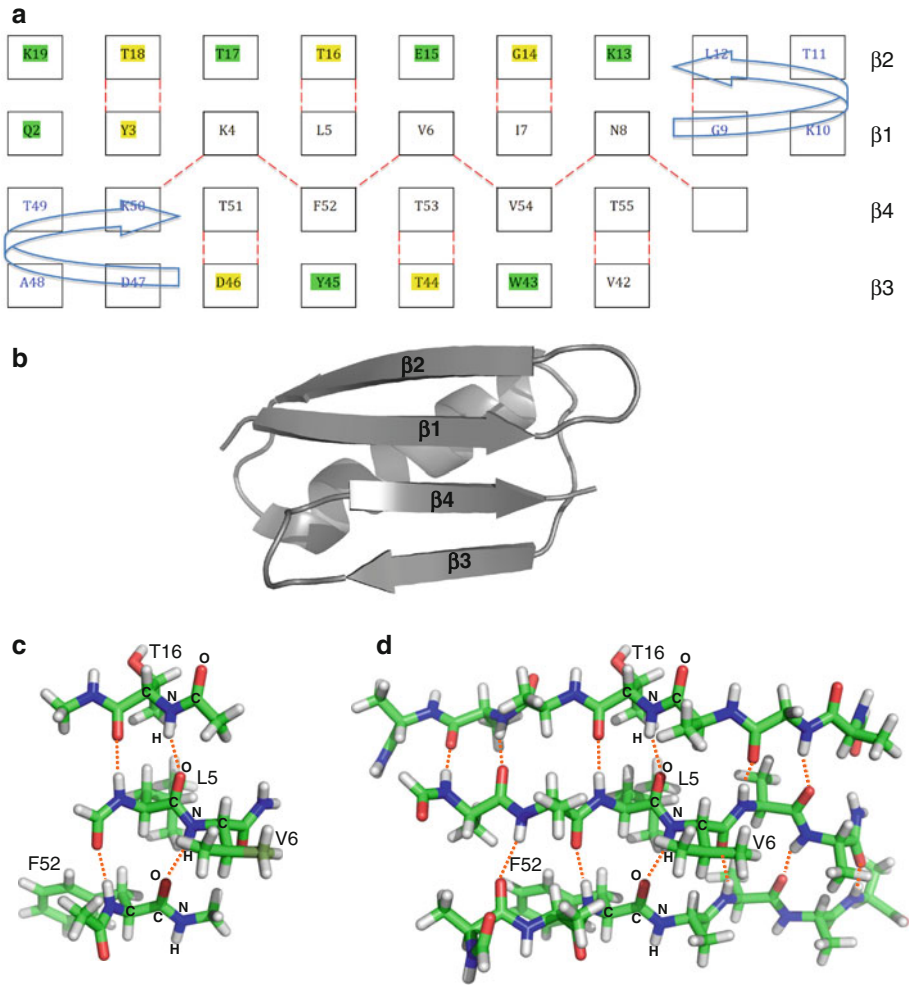

Fig. 1 **A** Schematic diagram of the β-sheet residues in GB3 illustrating the hydrogen bonding (*HB*) network. The *arrows* indicate the directions of the turns connecting the β-strands. Residues highlighted in *yellow* or *green* have a direct or an indirect HB partner only; those not highlighted have both direct and indirect HB partners. Turn residues are indicated by the *blue* numbers. The *empty box* represents E56 (not included in this study) which forms a HB with N8. Note that for a given residue *i*, the residue whose carbonyl oxygen forms a hydrogen bond with the amide N of residue *i* is considered a direct HB partner, whereas the residue whose amide N is hydrogen bonded to the carbonyl O of residue $i - 1$ is considered an indirect HB partner of residue *i*. **B** A ribbon representation of GB3's tertiary structure. Illustrations of **C** the fragment model and **D** the extended model used for ^{15}N shielding calculations for V6 (see "Computational methods"). All molecular fragments included in the calculations are shown in *stick* representation with standard atom coloring (C is *green*, N is *blue*, O is *red*, and H is *white*), the *dotted lines* indicate hydrogen bonds. Residues and the specific atoms that were assigned the 6–311 + G(2d,p) basis set are indicated; all other atoms in these models were assigned the less dense 4–21G basis set. All molecular drawings in this paper were prepared using PyMol (The PyMOL Molecular Graphics System, Version 1.2r1, Schrödinger, LLC.)

there is essentially no systematic offset in the ^{15}N shielding tensor values calculated here.

Isotropic shielding: comparison with experimental data

Encouraged by the agreement discussed above, we then examined how our results compare with the reported experimental values of the isotropic ^{15}N chemical shifts in GB3. In order to facilitate the comparison, we converted our calculated ^{15}N shielding values ($\sigma_{iso} = \mathrm{tr}\{\underline{\sigma}\}/3$) into chemical shifts, δ_{calc}, using the absolute ^{15}N shielding of liquid ammonia as the reference value, as recommended by IUPAC (Markley et al. 1998):

$$\delta_{calc} = 244.6\,\mathrm{ppm} - \sigma_{iso} \quad (1)$$

Several computer programs (SPARTA (Shen and Bax 2007), SHIFTX (Neal et al. 2003), SHIFTS (Xu and Case 2001; Xu and Case 2002) etc.) have been developed over the past decade to predict isotropic chemical shifts from a given sequence or structure of a molecular fragment, or, in reverse,

Table 1 Calculated isotropic ^{15}N shielding for β-sheet residues in GB3

Residue	Direct HB partner	Indirect HB partner	Fragment model	Neutral fragment model	CFP model	Extended model	Experiment (solid state)	Experiment (solution)
Q2		A20	111.16[a]		–[a]	–[a]	120.31	121.25
Y3	T18		119.06		108.89	117.71	124.16	120.31
K4	K50	T18	126.72	121.35	116.49	124.26	120.72	121.92
L5	T16	F52	109.73	112.77	110.48	110.73	117.82	117.95
V6	F52	T16	111.85		106.35	111.74	117.08	117.36
I7	G14	V54	110.11		116.21	110.98	118.69	118.96
N8	V54	G14	109.77		103.81	110.07	117.25	115.38
K13		G9	119.09	116.31	124.98	117.74	122.98	120.78
G14	I7		141.21	146.68	142.51	138.75	139.38	135.16
E15		I7	118.90	124.39	124.23	115.20	123.29	126.27
T16	L5		137.99	131.11	138.00	136.94	131.52	128.84
T17		L5	134.43		144.93	130.38	131.05	132.75
T18	Y3		133.78		139.53	130.55	129.62	129.36
K19		Y3	120.73	114.22	125.39	117.96	118.71	120.14
V42	T55		133.31		137.22	132.71	133.10	124.10
W43		T55	121.71		128.39	119.16	122.02	113.32
T44	T53		138.82		139.45	138.73	133.72	129.86
Y45		T53	124.81		124.54	123.43	127.60	124.37
D46	T51		102.97	117.16	113.61	104.34	118.35	116.14
T51	D46	K4	–[b]	128.04	118.45	128.60[c]	133.57	133.30
F52	K4	D46	116.65	113.41	115.54	116.65	114.17	113.22
T53	T44	V6	125.34		121.63	125.60	131.33	126.87
V54	V6	T44	117.83		114.31	118.48	124.99	121.33
T55	V42	N8	118.21		115.39	118.09	122.22	120.34

Shown for each β-sheet residue in GB3 are its direct and indirect hydrogen bonding partners and the isotropic ^{15}N shielding (σ_{iso}, in ppm) calculated using various models considered here: the fragment model (charged and neutral), the CFP model, and the extended model. The experimental data represent isotropic ^{15}N shielding values converted from the measured chemical shifts using ^{15}N shielding of liquid ammonia as the reference (see Eq. 1)

[a] For Q2, the fragment model calculation was performed using full basis set assignment, i.e. all atoms were assigned the basis set 6–311 + G(2d,p). Extended-model calculation could not be performed properly for Q2 because the sulfur atom (in the side chain of M1) was involved that cannot be assigned a 4–21G basis set in GAUSSIAN03

[b] For T51, fragment-model calculations including both direct and indirect HB partners could not be completed, because we were not able to converge to a sufficient accuracy the self-consistent iterations for the solution of Kohn–Sham equation

[c] The result shown here for T51 was obtained assuming a neutral form for its direct (D46) and indirect (K4) HB partners, as well as for K50

predict secondary and tertiary structure from chemical shifts (CSI (Wishart et al. 1992), TALOS (Cornilescu et al. 1999; Shen et al. 2009b), CS-ROSETTA (Shen et al. 2008; Shen et al. 2009a)). It is found that the correlation of these predicted shifts is high for C_α and C_β sites but poor for N_H and C'. Although these programs utilize a largely solution-state chemical shift database, these correlations mirror the relationships between the chemical shifts measured in solution versus solid state, where agreement is good for $^{13}C_\alpha$ and $^{13}C_\beta$, but poorer for ^{15}N and ^{13}C'. GB3 presents a suitable case for such a comparison since the experimental ^{15}N chemical shifts in solution (δ_{sol}) differ from those in solid state (δ_{cryst}) (Nadaud et al. 2007). This difference is most pronounced in the β-sheet residues, where it reaches 9 ppm and the RMSD of 3.5 ppm between δ_{sol} and δ_{cryst} is even greater than that between δ_{cryst} values in GB3 and GB1 (2.9 ppm for all β-sheet residues or 3.1 ppm if only identical residues are included). Thus, by comparing our predictions with both solution and solid-state data we expected to gain insights into possible effect of the environment (e.g. crystal packing) on ^{15}N chemical shifts. Therefore, as in the previous study, our comparison included experimental ^{15}N chemical shifts observed in solution, δ_{sol} (provided by Gabriel Cornilescu), as well as in microcrystals, δ_{cryst} (from solid-state NMR measurements (Nadaud et al. 2007).

Overall, the calculated isotropic ^{15}N chemical shifts show a reasonable correlation with the experimental data for GB3 (Fig. 3). Interestingly, however, our results

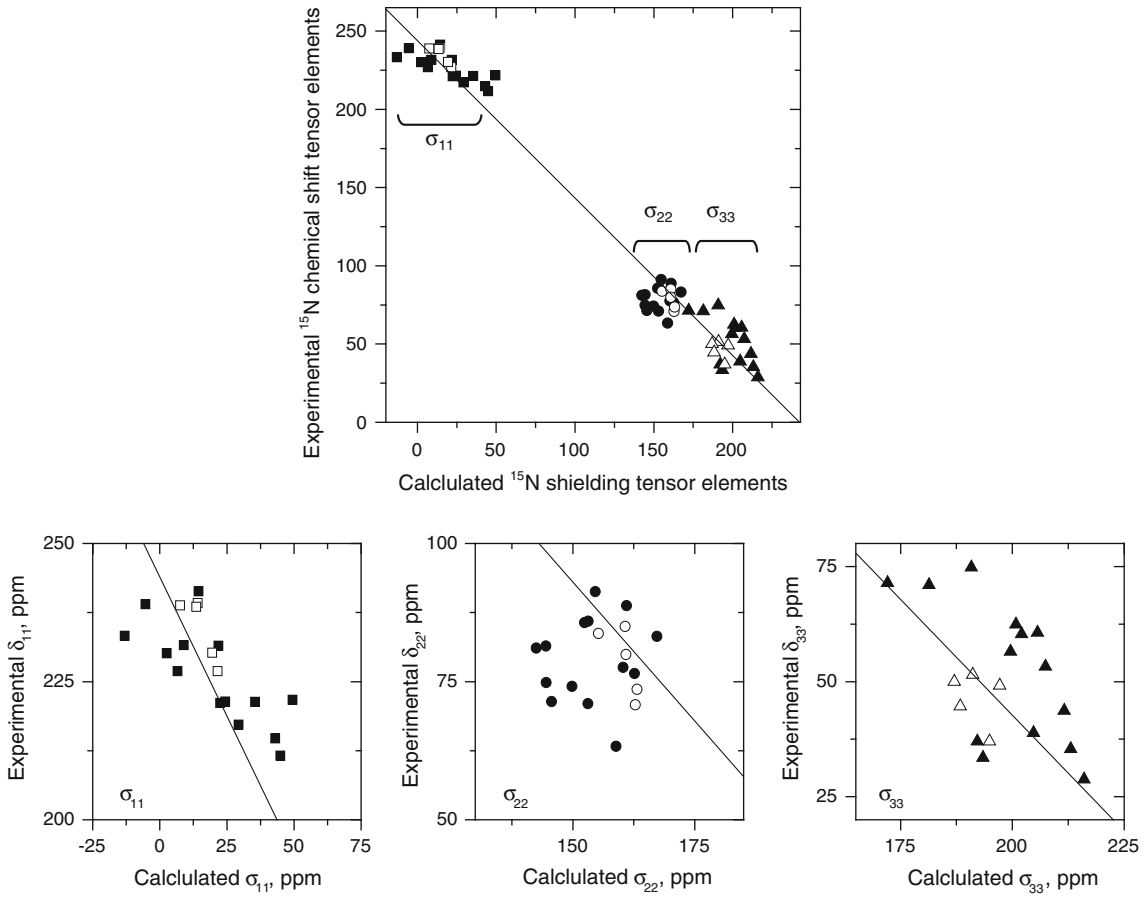

Fig. 2 The agreement of the principal components of the calculated ^{15}N shielding tensors for GB3 with the corresponding components of the experimental chemical shift tensors from slow magic angle spinning solid-state NMR measurements in GB1 microcrystals (Wylie et al. 2007). Shown are data (in ppm) for residues L5, G14-T18, A26-K28, K31, Y33, W43-D46, and F52-T55 which are shared by GB1 and GB3, and for which experimental data for GB1 are available. *Solid symbols* correspond to β-sheet residues while *open symbols* depict a similar comparison for the helical residues (included here for completeness, from (Cai et al. 2009)). *Squares*, *circles*, and *triangles* represent the principal components σ_{11}, σ_{22}, and σ_{33}, respectively. The Pearson's correlation coefficient (r) is -0.982 (for β-sheet) or -0.987 (β-sheet and α-helix). The parameters of the regression line are as follows: intercept $= 241.43 \pm 4.32$ ppm, slope $= -0.98 \pm 0.03$, for β-sheet residues only, or intercept $= 243.94 \pm 3.29$ ppm, slope $= -1.01 \pm 0.02$ when both β-sheet and α-helix data are analyzed together (shown as *solid line*). *Panels* on the *bottom* zoom on the individual components of the tensor, as indicated

correlate with solid-state NMR data better ($r = 0.88$) than with solution NMR data ($r = 0.82$). A close analysis shows that residues with the biggest discrepancy, $\Delta\delta = \delta_{sol} - \delta_{cryst}$, between experimental solution and solid-state ^{15}N chemical shifts are clustered primarily in the outer strands $\beta2$ and $\beta3$ and the adjacent turns (Fig. 3). It is also noteworthy that the high $\Delta\delta$ values ($|\Delta\delta| > 2.0$ ppm) in GB3's β-sheet residues are all positive (except for E15), indicating a stronger shielding effect in the solid state. Of these residues, V42 and W43 have the highest $\Delta\delta$ values of 9.0 and 8.7 ppm, respectively. Removing a single data point, W43, improves considerably ($r = 0.87$) the correlation with solution data, making it comparable to that with solid-state NMR data. Interestingly, the β-sheet residues with $|\Delta\delta| > 2.0$ ppm show a significantly better correlation with solid-state ($r = 0.93$) than with solution NMR data ($r = 0.79$; Fig. 3). In contrast, there is a smaller difference between the corresponding correlation coefficients ($r = 0.88$ and 0.83, respectively) for residues with $|\Delta\delta| < 2.0$ ppm.

The localization of high $|\Delta\delta|$ values points to possible differences between solution and crystals GB3 structures, likely involving the outer strands $\beta2$ and $\beta3$. In fact, an inspection of the crystal structure of GB3 (PDB code 1IGD (Derrick and Wigley 1994)) revealed close crystallographic contacts (possibly involving hydrogen bonds) between the $\beta3$ strand of one GB3 molecule and the $\beta2$ strand (plus the $\beta2/\beta3$ turn) of another (Fig. 3). (Note that similar contacts are also present in the two documented crystal forms of GB1(Gallagher et al. 1994).) Because the atom coordinates used in our calculations (PDB code 2OED (Ulmer et al. 2003)) were obtained by refinement of the crystal structure (1IGD) using backbone RDCs, the rotameric states of the side chains are essentially the same as in 1IGD (for

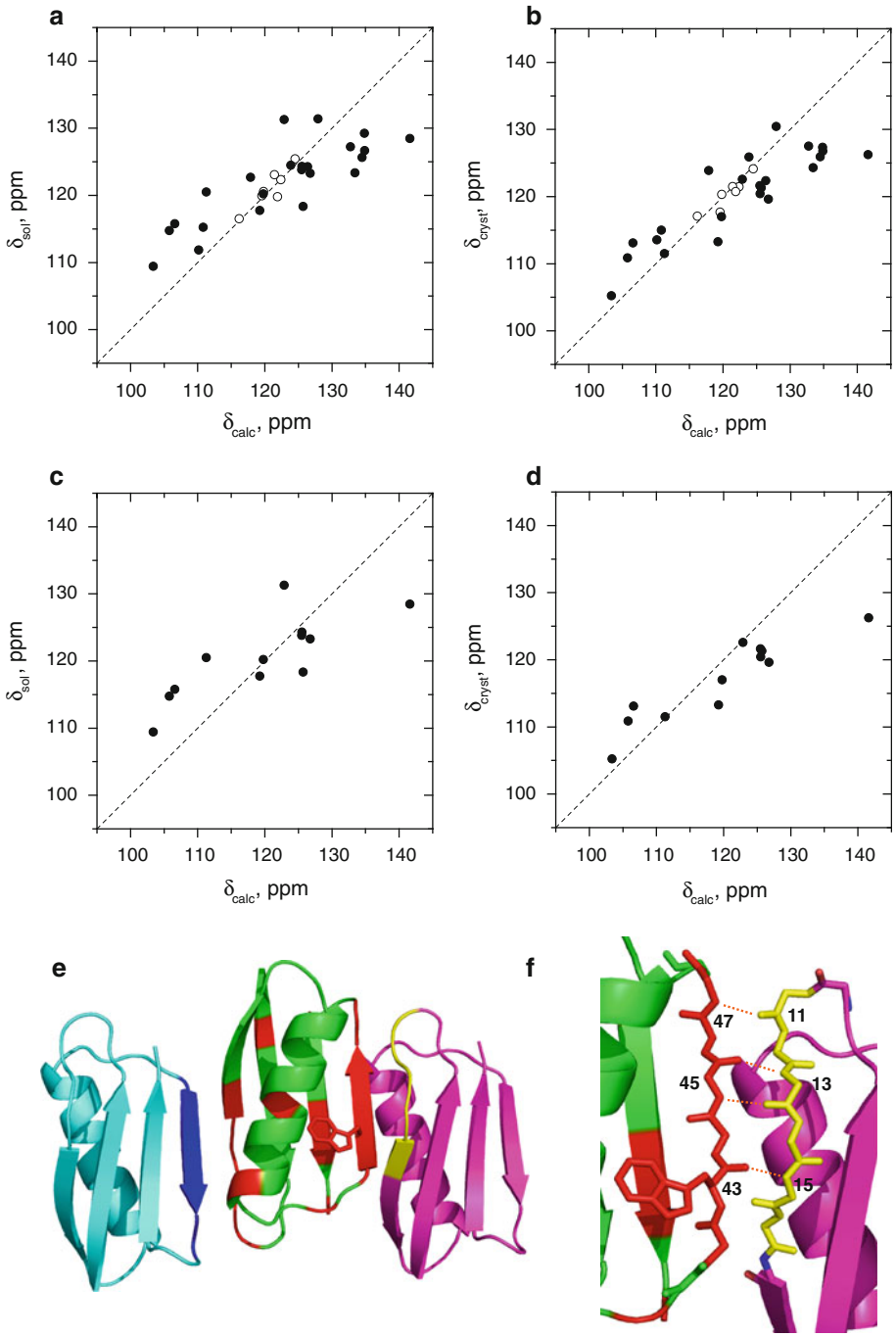

Fig. 3 Comparison of the isotropic ^{15}N chemical shifts calculated for the β-sheet residues in GB3 using the fragment model with the corresponding experimental chemical shifts **a** in solution and **b** in microcrystals (Nadaud et al. 2007). Also included are data for α-helical residues (*open circles*), for completeness. The Pearson's correlation coefficient between the calculated and experimental data for the β-sheet residues is 0.82 (**a**) and 0.88 (**b**). To guide the eye, the *dashed line* represents an ideal agreement. Panels **c**, **d** show a similar comparison for the subset of β-sheet residues whose ^{15}N chemical shifts differ by more than 2.0 ppm between solution and solid state. The correlation coefficients are 0.79 (**c**) and 0.93 (**d**). **e** Crystallographic contacts between a GB3 molecule (*green*) and its two neighbors (cyan and magenta) in the crystal. Residues with $|\Delta\delta| > 2.0$ ppm in the (*green*) GB3 molecule are colored *red*. The same residues (from the contacting strands) in the other two molecules are *colored blue* and *gold*. Also shown is the side chain of W43. **f** Zoom on the structure from panel **e** showing direct HB contacts between the β3 strand of one molecule and the β2 strand and the β1/β2 turn of its neighbor

example, the RMSD for χ_1 angles is 3.3°), and even the backbone dihedral angles are very similar (RMSD = 2.9° for ϕ and 4.5° for ψ). In fact, heavy atoms of the secondary structure elements in 2OED superimpose with those in 1IGD with the RMSD of 0.26 Å (all heavy atoms) or 0.23 Å (backbone); the corresponding numbers for the whole protein (residues 3–56) are 0.38 Å and 0.36 Å, respectively. Note that the backbone atom coordinates in 2OED are in almost perfect agreement with the RDCs measured in solution (Ulmer et al. 2003). The fact that our results, obtained using what essentially is the crystal structure of GB3, correlate better with measurements in microcrystals (1) suggests that the crystal contacts are responsible for the observed difference between solution and solid state ^{15}N chemical shifts (a similar observation was reported for GB1 (Franks et al. 2005)), (2) demonstrates the sensitivity of ^{15}N chemical shifts to rather subtle rearrangements (side chain conformations) in the protein structure, and (3) demonstrates that density functional calculations are capable of mirroring these differences. As our calculations

were based on the geometry in the X-ray crystal structure, these results also suggest that the structure and packing contacts in the microcrystals were similar to those in the X-ray study.

Conformational flexibility could be another possible reason for the difference in ^{15}N chemical shifts between solution and microcrystals, clustered primarily in the outer strands of GB3. In contrast to the inner strands (β1, β4), the outer strands, lacking HB contacts with a neighboring strand on one side, should experience lesser steric restrictions imposed by such contacts. Higher conformational flexibility of the outer strands would cause motional averaging of their chemical shift tensors. This would also possibly explain a somewhat lesser agreement between solution data and our calculations based on a single structure rather than a conformational ensemble. In fact, the backbone NH-bond order parameters, reflecting the amplitude of ps-ns motions, are on average somewhat lower in β2 ($S^2 = 0.80 \pm 0.04$) than in the inner strands β1 ($S^2 = 0.86 \pm 0.02$) and β4 ($S^2 = 0.86 \pm 0.03$; Hall and Fushman 2003). Additional motions (on a ms-μs time scale) in the β2 strand appear also substantiated by large R_{ex} terms observed at reduced temperatures (Yao et al. 2010). However, strand β3 containing residues with the highest $\Delta\delta$ does not exhibit higher flexibility ($S^2 = 0.85 \pm 0.02$). A similar tendency is observed in the RDC-derived order parameters (Bernado and Blackledge 2004; Clore and Schwieters 2004; Yao et al. 2010) that reflect amplitudes of motions on a slower time scale, up to milliseconds. Thus, we conclude that it is less likely that the observed large $|\Delta\delta|$ values are due to dynamic averaging of ^{15}N chemical shifts in solution.

Although our calculated chemical shifts show a fairly good correlation with experimental data, some differences still remain. In order to gain insights into possible reasons for the observed differences and to explore various ways of improving the agreement with experiment, we perfomed calculations using more complex structural and physical models, as outlined below.

Extended model: The effect of including entire β-strands

One possible reason for the less than ideal agreement with experimental data is that our fragment models might not have included enough close contacts. In fact, by its very nature, a β-strand is accompanied by and hydrogen bonded with other β-strand(s) in a parallel or antiparallel fashion (also see Fig. 1). In an earlier paper (Xu and Case 2002), a model for calculating shieldings in a β-sheet was designed as a 3–5 residue sequence (containing the residue of interest) along with two β-strands running on both sides. Obviously, by including more neighboring groups in close contact, such a model would have more interactions (e.g. electrostatic effects) taken into account. As an example from our calculation (not shown) for T17, bringing an additional residue (K4) into the model resulted in a 6 ppm deshielding. In this case, K4 is neither directly nor indirectly hydrogen bonded with T17 but rather opposes T17 from a neighboring strand. Interestingly, however, modifying the side chain of K4 to be neutral yields similar results (see below) so it is not the charge of K4 per se that caused this effect.

Therefore we repeated the calculations for all β-sheet residues using the *extended* model, which included all residues in the current strand and its immediate neighboring strand(s) (see "Computational methods"). The results are shown in Table 1. Somewhat surprisingly, the extended model calculations only slightly modified the fragment model results. The RMSD between the results of the two models is 1.92 ppm, the correlation coefficient is 0.99. Extending the fragments to full-length strands deshielded ^{15}N on average by 0.98 ppm (standard deviation 1.69 ppm). The agreement with experiment for the extended model was almost the same as for the fragment model: $r = 0.89$ (solid state data) and 0.82 (solution data). These results indicate that most of the neighbor-contact interactions were already included in the fragment model. Note that in order to account for the neutralizing effect of counterions, the carboxy-terminus of E56 was replaced by the formyl group (COH). Our calculations show that keeping the C-terminus in its deprotonated/charged form (i.e. as COO^-) has little effect on the calculated shieldings, except for residues N8, W43, V54, and T55, which are within 10 Å from the C-terminal oxygens (see Supplementary Table S3). For three of these residues the agreement with experiment became worse, and only for W43 we observed a slight improvement in the agreement with solid-state but not solution NMR data.

The effect of side chain charges

The charge state of side chains can have a profound effect on ^{15}N chemical shifts of an ionizable residue as well as its neigbors (see e.g. (Poon et al. 2004; Cai et al. 2008)). As discussed in our previous paper (Cai et al. 2009), in GB3's α-helix the charged side chains are located such that they form salt bridges with the oppositely charged side chains from the same helix, and therefore naturally balance each other's charges. Thus, it was not necessary to neutralize those side chains. In the case of β-sheet residues, there is a salt bridge between K4 and E15 (as well as between D47 and K50 in the β3/β4 turn), while the charges of the other relevant ionizable side chains (K13, K19, D46) could be shielded/balanced by the counterions present in the buffer. Note that all these side chains are solvent exposed. Since

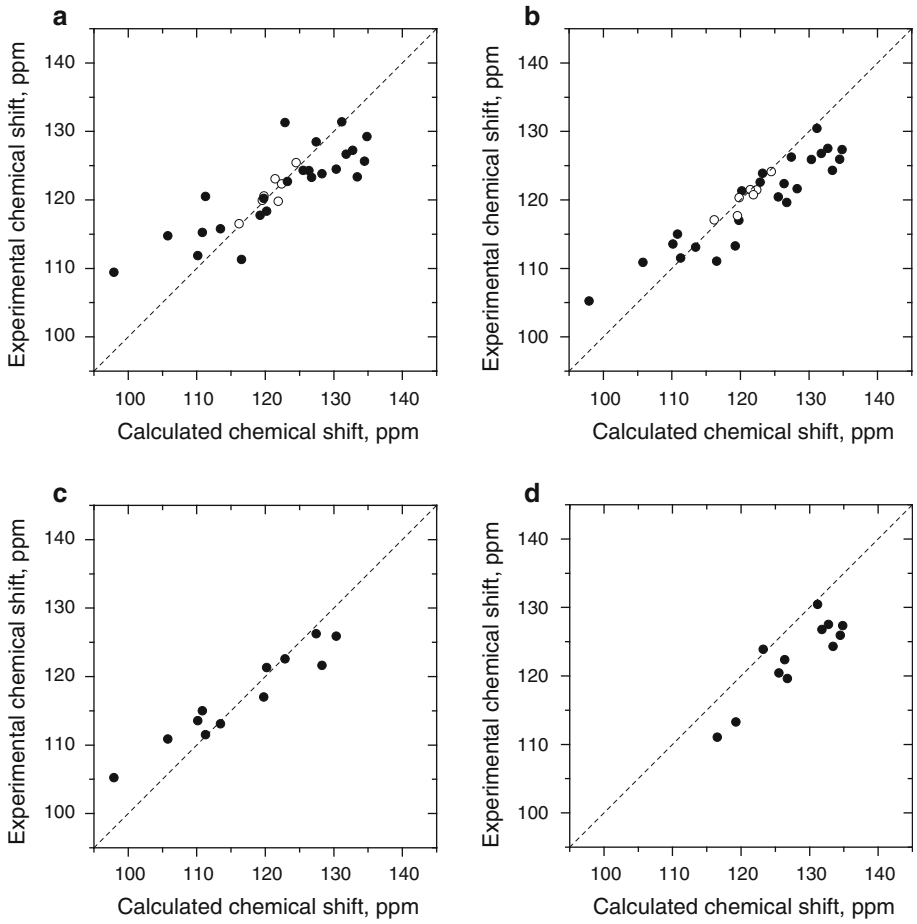

Fig. 4 Comparison of the isotropic ^{15}N chemical shifts calculated for the β-sheet residues in GB3 using the neutral fragment model with the corresponding experimental chemical shifts measured **a** in solution and **b** in microcrystals (Nadaud et al. 2007). The correlation coefficients are 0.86 **a** and 0.93 **b**. **c**, **d** The comparison with solid-state data (from **b**) is split into two groups: residues located in the outer strands (**c** $r = 0.96$) and inner strands (**d** $r = 0.82$). While the outer-strand residues show an overall good agreement with experimental data ($\delta_{calc} - \delta_{cryst} = -0.45 \pm 4.1$ ppm, RMSD = 3.9 ppm), for the inner-strand residues the calculated chemical shifts appear systematically overestimated by 5.3 ppm on average (std = 2.9 ppm), or by 6.3 ppm (std = 1.7 ppm) when excluding the two residues (K4, F52) for which the agreement is almost perfect

no counterions are explicitly included in our calculation, we thought that a good approximation would be to include them implicitly by considering all relevant ionizable side chains in their neutral form. This modification is expected to affect the results for residues K4, L5, K13, G14, E15, T16, K19, D46, and F52. To examine the effect, we performed ^{15}N shielding calculations (Table 1) for these residues using a neutral form for all side chains in the corresponding fragments (referred further as the *neutral-fragment* model). Indeed, making ionizable side chains neutral improved the correlation with experiment for the abovementioned residues: the correlation coefficient with the solid-state data increased from 0.84 to 0.96, and with solution NMR from 0.84 to 0.93. This also further improved the overall agreement between the calculation and experiment for β-sheet residues (Fig. 4), resulting in $r = 0.93$ and 0.86, respectively, for solid-state and solution NMR data. This modification had the biggest effect on D46, where it produced a strong shielding by 14.2 ppm. The rest of the affected residues experienced either shielding or deshielding, with the magnitude of the effect ranging from 2.8 to 6.9 ppm (mean = −1.3 ppm, standard deviation 5.3 ppm). Interestingly, we obtained a significantly better correlation with experiment (solid-state NMR; Fig. 4) for the outer strands ($r = 0.96$) than for the inner strands ($r = 0.82$). A similar trend was observed in the results for the fragment model, where the corresponding numbers are 0.91 and 0.64, respectively. The reasons for this are not clear.

Charge field perturbations calculations: the effect of charges from the rest of the protein

As a next step toward taking into account all possible contributions to ^{15}N shielding, we assessed the effect of the charges of the atoms from the rest of the protein, that were not included in the calculations by means of explicit atomic models discussed above. For this purpose we performed CFP calculations in which those atoms were represented by point charges, as detailed elsewhere (Cai et al. 2009). The results are shown in Table 1.

Interestingly, the inclusion of point charges from the rest of the protein increased (compared to the fragment model) ^{15}N shielding for practically all residues in the outer strands (except for T16 and Y45, which remained essentially unperturbed), whereas the majority of residues in the

inner strands experienced deshielding. The magnitude of the observed difference, $\Delta\delta_{CFP}$, between the CFP and fragment-model results ranged from 0 to 10.6 ppm. As discussed in the case of α-helical residues (Cai et al. 2009), smaller $\Delta\delta_{CFP}$ values indicate that we have included enough close groups in the fragment-model calculation and give more confidence in the results. Indeed, a better correlation with experiment is seen for those residues whose $\Delta\delta_{CFP}$ values are small: e.g., $r = 0.92$–0.93 for residues with $\Delta\delta_{CFP} < 3$ ppm in contrast with $r = 0.75$ (solution data) or 0.83 (solid state data) for residues with $\Delta\delta_{CFP} > 3$ ppm. For those residues with big $\Delta\delta_{CFP}$, there is still room for improvement of the calculations by including additional charges from the rest of the protein.

Chemical shift calculations for β-turn residues

We also performed ^{15}N shielding calculations for residues G9-L12 and D47-K50 located in the $\beta1/\beta2$ and $\beta3/\beta4$ turns connecting the corresponding β-strands. In the $\beta1/\beta2$ turn, only G9 has a direct HB partner (L12), while the only ionizable side chain (K10) is solvent exposed such that its ε-amino group is distant from the rest of the residues. The interaction network in the $\beta3/\beta4$ turn is more complex: here D47 has an indirect HB partner (T51), while the NH of T49 could form a HB with the side chain $O_{\delta1}$ of D46. Moreover, the side chains of D47 and K50 form a salt bridge, while the side chain of D46 is in close proximity to all amides in this turn, such that its ionization state could have a strong effect on the ^{15}N chemical shifts. Therefore, when building the fragment models for the turn residues, we started with the smallest, 2-residue fragment (i, $i-1$), and continued including adjacent residues until the fragment contained the entire turn and beyond (see Table 2). Thus, in the case of the $\beta3/\beta4$ turn, it was also necessary to include D46 for all residues. For example, the isotropic ^{15}N shielding of A48 calculated for the shortest fragment (D47-A48) was 141.3 ppm and did not change upon addition of T49 (141.6 ppm); however, adding T49 and K50 reduced it to 132 ppm, and subsequent inclusion of D46 reduced it further to 114.6 ppm. Making D46 neutral increased the shielding only slightly (121.2 ppm), indicating that it is not only the charge but also the side chain of D46 per se, that makes the difference here. In accordance with the structural and distance considerations mentioned above, while the ionization state of D46 has a profound effect on ^{15}N shifts of several residues in the $\beta3/\beta4$ turn (Fig. 5), neutralizing K10 affected essentially only its own ^{15}N chemical shift (see Table 2).

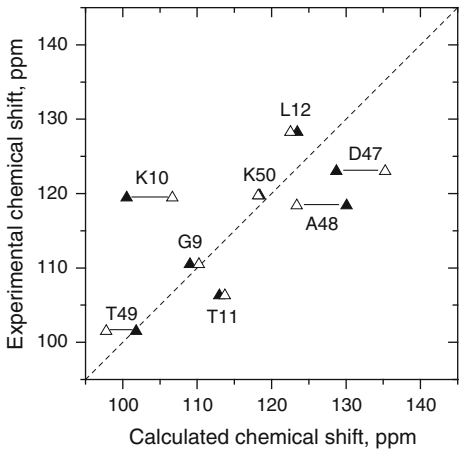

Fig. 5 Comparison of the isotropic ^{15}N chemical shifts calculated for the turn residues in GB3 using the fragment model (*solid triangles*) or the neutral fragment model (*open triangles*) with the corresponding experimental chemical shifts measured in GB3 microcrystals (Nadaud et al. 2007). Data for the same residue are connected by a *horizontal line*

The results of our calculations are summarized in Table 2 and Supplementary Table S2. Overall, the calculated chemical shifts for the turn residues generally

Table 2 Calculated isotropic ^{15}N shielding for the β-turn residues in GB3

Residue	Fragment model	Neutral fragment	Experiment solid state	Experiment solution	Residues included
G9	135.55	134.36	134.13	134.12	N8, G9, K10*, T11, L12
K10	144.05	137.93	125.18	123.74	G9, K10*, T11, L12
T11	131.62	130.87	138.31	135.60	G9, K10*, T11, L12
L12	121.13	122.07	116.33	118.71	G9, K10*, T11, L12
D47	115.90	109.33	121.61	119.53	D46*, D47, A48, T49, K50, T51
A48	114.55	121.21	126.22	124.61	D46*, D47, A48, T49, K50
T49	142.81	146.81	143.10	141.30	D46*, D47, A48, T49, K50
K50	126.17	126.40	124.87	121.38	D46*, D47, A48, T49, K50

Shown for each turn residue in GB3 are the isotropic ^{15}N shielding (σ_{iso}, in ppm) calculated using two extended-fragment models (charged and neutral) and the residues included in the fragment. The asterisk indicates residues (K10, D46) that were assumed neutral in the neutral fragment calculations. The experimental data represent isotropic ^{15}N shielding values converted from the measured chemical shifts using ^{15}N shielding of liquid ammonia as the reference (see Eq. 1)

correlate with the experimental data (Fig. 5). The somewhat greater discrepancy between the calculation and experiment could in part be due to greater conformational flexibility (disorder) in the turns (Hall and Fushman 2003).

Discussion and Conclusions

We performed ^{15}N shielding calculations for all twenty-four β-sheet residues and eight turn residues of the protein GB3 both in vacuum (for various structural and charges models) and using the CFP method. We found a good correlation between the individual components of the ^{15}N shielding tensor and the experimental data. Comparing the isotropic chemical shifts with experiment, we observed a slightly better overall correlation with solid-state NMR data, obtained in microcrystals, than with solution NMR data. A possible reason for this is close crystallographic contacts between neighboring molecules in the crystals, reflected in the difference between the experimental data themselves. As the result, for those residues with the larger chemical shift difference between solution and microcrystals, the calculations (based on the crystal structure) agree better with solid-state NMR data. We analyzed the effect of including additional residues/groups in the model and the effect of charges on the neighboring side chains as well as of the rest of the protein. Increasing the length of molecular fragments by including entire β-strands did not substantially change the results. We showed however that considering the neutral form of ionisable side chains improves further the agreement with experiment. We also found that those residues with a smaller difference between the vacuum and CFP calculations tend to have a better correlation with experimental data when using the vacuum results. This reinforces the message that the CFP calculation can help determine whether or not the size of the fragment is large enough to take interprotein electrostatic interactions into account.

Figure 6 summarizes the comparison with experiment for all calculated ^{15}N chemical shifts (α-helix, β-sheet, and turns) covering 71% of GB3 residues. Despite the encouraging correlation, the density functional calculations are not yet at the level where we could predict ^{15}N shifts with the accuracy comparable to experimental precision. Thus, the RMSDs between the calculated ^{15}N chemical

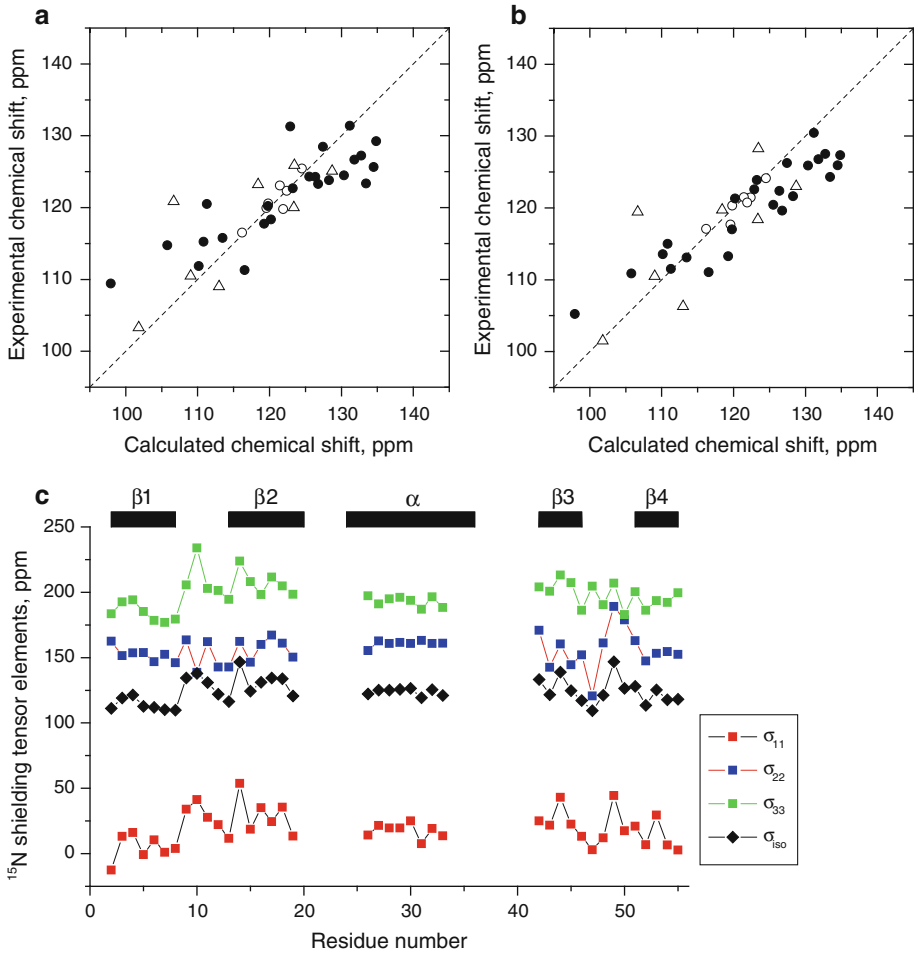

Fig. 6 Summary of the agreement between the isotropic ^{15}N chemical shifts calculated for the 39 residues in GB3 (neutral fragment model) and the corresponding experimental chemical shifts measured in **a** solution and **b** GB3 microcrystals (Nadaud et al. 2007). Shown are data for the β-sheet (*solid circles*), α-helix (*open circles*), and turns $\beta1/\beta2$ and $\beta3/\beta4$ (*open triangles*). **c** Principal components of the calculated ^{15}N shielding tensor as a function of residue number in GB3, colored *red* (σ_{11}), *blue* (σ_{22}), and *green* (σ_{33}). Also shown is the isotropic shielding (*black*)

shifts and the experimental data (solid state) are 5.0 ppm for the β-sheet, 6.0 ppm for the β-turns, and 1.0 ppm for the α-helix. The corresponding numbers for solution NMR data are 5.7 ppm (β-sheet), 5.9 ppm (β-turns), and 1.1 ppm (α-helix).

Our results raise several questions that need to be addressed by future calculations:

1. What is the reason for the apparently good correlation with experiment and the lack of agreement for the actual values of the chemical shifts in the β-sheet and the turns? Why is the prediction for the α-helix so much more accurate?
2. Although the isotropic shifts/shieldings correlate well with experiment, the individual components of the shielding tensor do not show the same level of correlation. We find that the σ_{11} and σ_{33} components show a noticeable correlation with solid state NMR data for GB1 ($r = -0.78$ and -0.61, respectively) in the β-sheet, and therefore likely are responsible for the observed correlation with the isotropic shifts. At the same time, the σ_{22} component of the tensor shows practically no correlation ($r = 0.12$). This is also reflected in the RMSDs between the predicted and experimental values: 13.0, 16.4, and 13.9 ppm for σ_{11}, σ_{22} and σ_{33}, respectively. However, in the α-helix it is the σ_{11} and σ_{22} components that show most correlation ($r = -0.88$ and -0.71), while σ_{33} appears uncorrelated ($r = -0.29$). A similar tendency is seen in the β-turns, where the corresponding correlation coefficients are -0.60, -0.71, and 0.37 (for σ_{11}, σ_{22}, and σ_{33}). Note that the sensitivity of the intermediate, σ_{22}, component to the backbone conformation has also been observed in solid-state NMR studies of peptides reviewed in (Saito et al. 2010). This seems counter-intuitive, as all three components of the tensor could be interdependent. What could be the physical reason for such differential behavior of the tensor components?

Mirroring the discrepancies in the individual tensor components, the anisotropies of the predicted ^{15}N shielding tensors show little or no correlation with the available experimental data (Supplementary Figure S1). For example, comparison with the CSA values for GB1 (from solid state NMR measurements) yields correlation coefficients of 0.40 (β-sheet) and 0.48 (turns); although the correlation is quite good ($r = 0.88$) for the few residues in the α-helix that are the same in GB1 and GB3. The correlation with ^{15}N CSAs derived from residual chemical shift anisotropy studies (Yao et al. 2010) or from ^{15}N relaxation measurements at five magnetic fields (Hall and Fushman 2006) is also poor (Supplementary Figure S1).

Knowledge of the ^{15}N CSA values is critical for accurate determination of protein dynamics from ^{15}N relaxation measurements, as the CSA contribution to ^{15}N relaxation rates is substantial and increases as square of the magnetic field (see e.g.(Fushman et al. 1999; Hall and Fushman 2006)). As shown in (Fushman and Cowburn 2001; Hall and Fushman 2006), the model-free parameters derived from ^{15}N relaxation rates are directly affected by the input ^{15}N CSA values. Recent ^{15}N CSA measurements in GB3 (Yao et al. 2010) as well as solid state NMR data for GB1 returned higher (by absolute value) CSAs in the helix than in the β-sheet. In contrast, the calculated ^{15}N CSA values for the α-helix (-159.40 ± 4.54 ppm) are only slightly higher on average than for the rest of the protein: -155.11 ± 6.72 ppm in the turns and -158.23 ± 10.73 in the β-sheet. Moreover, the calculated CSAs for the β-sheet show a significant variation from residue to residue, as well as among the β-strands: -163.86 ± 11.12 ppm (β1), -154.35 ± 11.06 ppm (β2), -153.06 ± 6.99 ppm (β3); and -160.93 ± 10.94 ppm (in β4). Note that a similar trend is present in the CSA values derived from ^{15}N relaxation measurements in GB3 (Hall and Fushman 2006) and ubiquitin (Fushman et al. 1998; Fushman et al. 1999), where helical residues had very little spread in the CSA values, and these CSAs were not noticeably higher on average than in the β strands.

3. We notice that despite a reasonable correlation between the calculated and experimental isotropic chemical shifts, the actual slope of the regression lines (experiment versus calculation) in Figs. 3 and 4 differs from 1 for the β-sheet but is close to 1 for the α-helix. In fact, for the β-sheet residues, the slope is 0.53 ± 0.07 in Fig. 4a and 0.63 ± 0.06 in Fig. 4b; the corresponding numbers for the α-helical residues are 0.98 ± 0.20 and 0.84 ± 0.15, respectively. Nominally this indicates a bigger shielding range produced by the calculation (36.9 ppm) than that observed experimentally (21.9 ppm in solution and 25.2 ppm in microcrystals) for the β-sheet residues. As measurement errors are generally expected to increase the degree of variation observed in experiment, this result could reflect the effect of "structural noise" or attenuation of extreme calculated values by internal motions. Because the atom coordinates used in our calculations were already refined based on experimental RDC data, we can speculate that a possible physical reason for the observed discrepancy could be motional averaging of experimental chemical shifts by the backbone and side chain dynamics in the protein. In fact, both ^{15}N relaxation (Hall and Fushman 2003) and RDC (Bernado and Blackledge 2004) data suggest a somewhat more restricted local backbone dynamics in the α-helix compared to the rest of the protein in GB3. Note also that it has previously been suggested that the

poorly described χ torsion angles of the side chains are responsible for less satisfactory agreement between experimental and quantum mechanical theoretical chemical shifts for both C_α and C_β (Villegas et al. 2007). The arguments hold similarly for ^{15}N as (Le and Oldfield 1996) already demonstrated the effects of χ_1 torsion angles of the residues i and $i-1$ on the ^{15}N chemical shielding of residue i. Obviously, calculations using a single-structure model cannot represent the conformational variability and the effect of dynamic averaging within the structural ensemble of a protein. ^{15}N shielding calculations taking into account the conformational ensemble of GB3 structures will be required to address this issue.

It should be mentioned here that our calculations did not include water molecules as HB partners for the solvent-exposed carbonyls or amides. Although it is natural to expect that these groups would have the tendency to form hydrogen bonds with water in solution, the positions of the corresponding water molecules for GB3 were not well defined. For example, of the twelve solvent-exposed backbone CO or NH groups in the outer strands $\beta2$ and $\beta3$, only N of W43 has a water molecule properly positioned to form a hydrogen bond in the crystal structure of GB3 (1IGD). In the absence of experimentally well-defined positions for HB waters, we preferred not to position them arbitrarily and therefore did not include them in this study. Moreover, our calculation for W43 shows that the effect of the hydrogen-bonded water molecule on its ^{15}N shielding is rather small: including that water molecule reduced the isotropic shielding by only 0.25 ppm. Rigorous positioning of HB-partner water molecules and proper account for the solvent effect on ^{15}N shielding is expected to make the computational model more realistic and likely further improve the agreement with experiment. As we showed earlier in a model calculation (Cai et al. 2008), this could require hydrogen bonding to explicit water molecules in the first solvation shell combined with the polarizable continuum model for the remaining (bulk) solvent.

Other possible reasons for the observed less than perfect agreement with experiment are deficiencies in the quantum mechanical model (basis sets, particular choice of functionals for the DFT calculations, the lack of explicit electron-elecron correlations), the limitations in the number of atoms included in the calculations (in fact, for several residues the CFP results differ from those using the fragment model, indicating that not all important interactions are accounted for in the latter), and the limited statistics of the data analyzed here. Detailed further calculations for this and other proteins are necessary in order to obtain better statistics and potentially improve the computational models.

Acknowledgments Supported by NIH grant GM065334 to DF and Francqui Foundation to DSK. We thank Gabriel Cornilescu, Chad Rienstra, and Ben Wylie for making available detailed experimental chemical shift data for comparison and Christopher Jaroniec for insightful discussions.

References

Becke AD (1988) Density-functional exchange-energy approximation with correct asymptotic behavior. Phys Rev A 38(6):3098–3100

Becke AD (1993) Density-functional thermochemistry. III. The role of exact exchange. J Chem Phys 98:5648–5652

Bernado P, Blackledge M (2004) Local dynamic amplitudes on the protein backbone from dipolar couplings: toward the elucidation of slower motions in biomolecules. J Am Chem Soc 126(25): 7760–7761

Brender JR, Taylor DM, Ramamoorthy A (2001) Orientation of amide-nitrogen-15 chemical shift tensors in peptides: a quantum chemical study. J Am Chem Soc 123(5):914–922

Cai L, Fushman D, Kosov DS (2008) Density functional calculations of 15 N chemical shifts in solvated dipeptides. J Biomol NMR 41(2):77–88

Cai L, Fushman D, Kosov DS (2009) Density functional calculations of chemical shielding of backbone 15 N in helical residues of protein G. J Biomol NMR 45(3):245–253

Clore GM, Schwieters CD (2004) Amplitudes of protein backbone dynamics and correlated motions in a small alpha/beta protein: correspondence of dipolar coupling and heteronuclear relaxation measurements. Biochemistry 43(33):10678–10691

Cornell WD, Cieplak P, Bayly CI, Gould IR, Merz KM, Ferguson DM, Spellmeyer DC, Fox T, Caldwell JW, Kollman PA (1995) A second generation force-field for the simulation of proteins, nucleic acids, and organic molecules. J Am Chem Soc 117:5179–5197

Cornilescu G, Delaglio F, Bax A (1999) Protein backbone angle restraints from searching a database for chemical shift and sequence homology. J Biomol NMR 13(3):289–302

de Dios AC, Pearson JG, Oldfield E (1993) Secondary and tertiary structural effects on protein NMR chemical shifts: an ab initio approach. Science 260(5113):1491–1496

Derrick JP, Wigley DB (1994) The third IgG-binding domain from streptococcal protein G. An analysis by X-ray crystallography of the structure alone and in a complex with Fab. J Mol Biol 243(5):906–918

Franks WT, Zhou DH, Wylie BJ, Money BG, Graesser DT, Frericks HL, Sahota G, Rienstra CM (2005) Magic-angle spinning solid-state NMR spectroscopy of the beta1 immunoglobulin binding domain of protein G (GB1): 15 N and 13C chemical shift assignments and conformational analysis. J Am Chem Soc 127(35):12291–12305

Frisch M, Trucks G, Schlegel H, Scuseria G, Robb M, Cheeseman J, Montgomery J, Vreven T, Kudin K, Burant J, Millam J, Iyengar S, Tomasi J, Barone V, Mennucci B, Cossi M, Scalmani G, Rega N, Petersson G, Nakatsuji H, Hada M, Ehara M, Toyota K, Fukuda R, Hasegawa J, Ishida M, Nakajima T, Honda Y, Kitao O, Nakai H, Klene M, Li X, Knox J, Hratchian H, Cross J, Adamo C, Jaramillo J, Gomperts R, Stratmann R, Yazyev O, Austin A, Cammi R, Pomelli C, Ochterski J, Ayala P, Morokuma K, Voth G, Salvador P, Dannenberg J, Zakrzewski V, Dapprich S, Daniels A, Strain M, Farkas O, Malick D, Rabuck A, Raghavachari K, Foresman J, Ortiz JQ, Baboul A, Clifford S, Cioslowski J, Stefanov B, Liu G, Liashenko A, Piskorz P, Komaromi I, Martin R, Fox D, Keith T, Al-Laham M, Peng C,

Nanayakkara A, Challacombe M, Gill P, Johnson B, Chen W, Wong M, Gonzalez C, Pople J (2004) Gaussian 03, Revision C.02. Gaussian, Inc, Wallingford, CT

Fushman D, Cowburn D (2001) Nuclear magnetic resonance relaxation in determination of residue-specific 15 N chemical shift tensors in proteins in solution: protein dynamics, structure, and applications of transverse relaxation optimized spectroscopy. Methods Enzymol 339:109–126

Fushman D, Tjandra N, Cowburn D (1998) Direct measurement of ^{15}N chemical shift anisotropy in solution. J Am Chem Soc 120(42):10947–10952

Fushman D, Tjandra N, Cowburn D (1999) An approach to direct determination of protein dynamics from 15 N NMR relaxation at multiple fields, independent of variable 15 N chemical shift anisotropy and chemical exchange contributions. J Am Chem Soc 121:8577–8582

Gallagher T, Alexander P, Bryan P, Gilliland GL (1994) Two crystal structures of the B1 immunoglobulin-binding domain of streptococcal protein G and comparison with NMR. Biochemistry 33(15):4721–4729

Hall JB, Fushman D (2003) Characterization of the overall and local dynamics of a protein with intermediate rotational anisotropy: Differentiating between conformational exchange and anisotropic diffusion in the B3 domain of protein G. J Biomol NMR 27(3):261–275

Hall JB, Fushman D (2006) Variability of the 15 N chemical shielding tensors in the B3 domain of protein G from 15 N relaxation measurements at several fields. Implications for backbone order parameters. J Am Chem Soc 128(24):7855–7870

Harris RK, Becker ED, De Menezes SM, Granger P, Hoffman RE, Zilm KW (2008) Further conventions for NMR shielding and chemical shifts (IUPAC Recommendations 2008). Magn Reson Chem 46(6):582–598

Hiyama Y, Niu C, Silverton JV, Bavoso A, Torchia DA (1988) Determination of 15 N chemical shift tensor via 15 N–2H dipolar coupling in Boc-glycylglycyl[15 N glycine]benzyl ester. J Am Chem Soc 110:2378–2383

Jameson CJ, Jameson AK, Oppusunggu D, Wille S, Burrell PM, Mason J (1981) 15 N nuclear magnetic shielding scale from gas-phase studies. J Chem Phys 74:81–88

Le HB, Oldfield E (1996) Ab initio studies of amide-N-15 chemical shifts in dipeptides: applications to protein NMR spectroscopy. J Phys Chem 100:16423–16428

Lee DK, Ramamoorthy A (1998) A simple one-dimensional solid-state NMR method to characterize the nuclear spin interaction tensors associated with the peptide bond. J Magn Reson 133(1): 204–206

Lee C, Yang W, Parr RG (1988) Development of the Colle-Salvetti correlation-energy formula into a functional of the electron density. Phys Rev B Condens Matter 37(2):785–789

Lee D-K, Wei Y, Ramamoorthy A (2001) A Two-dimensional magic-angle decoupling and magic-angle turning solid-state NMR method: an application to study chemical shift tensors from peptides that are nonselectively labeled with 15 N isotope. J Phys Chem B 105(20):4752–4762

Lipsitz RS, Tjandra N (2003) 15 N chemical shift anisotropy in protein structure refinement and comparison with NH residual dipolar couplings. J Magn Reson 164(1):171–176

Markley JL, Bax A, Arata Y, Hilbers CW, Kaptein R, Sykes BD, Wright PE, Wuthrich K (1998) Recommendations for the presentation of NMR structures of proteins and nucleic acids. IUPAC-IUBMB-IUPAB Inter-union task group on the standardization of data bases of protein and nucleic acid structures determined by NMR spectroscopy. J Biomol NMR 12(1):1–23

Nadaud PS, Helmus JJ, Jaroniec CP (2007) C-13 and N-15 chemical shift assignments and secondary structure of the B3 immunoglobulin-binding domain of streptococcal protein G by magic-angle spinning solid-state NMR spectroscopy. Biomol NMR Assign 1:117–120

Neal S, Nip AM, Zhang H, Wishart DS (2003) Rapid and accurate calculation of protein 1H, 13C and 15 N chemical shifts. J Biomol NMR 26(3):215–240

Oas TG, Hartzell CJ, Dahlquist FW, Drobny GP (1987) The amide nitrogen-15 chemical shift tensors of four peptides determined from carbon-13 dipole-coupled chemical shift powder patterns. J Am Chem Soc 109:5962–5966

Oldfield E (1995) Chemical shifts and three-dimensional protein structures. J Biomol NMR 5(3):217–225

Poon A, Birn J, Ramamoorthy A (2004) How does an amide-N chemical shift tensor vary in peptides? J Phys Chem B 108(42):16577–16585

Ramamoorthy A, Wu CH, Opella SJ (1995) Three-dimensional solid-state NMR experiment that correlates the chemical shift and dipolar coupling frequencies of two heteronuclei. J Magn Reson B 107(1):88–90

Sadqi M, Fushman D, Munoz V (2006) Atom-by-atom analysis of global downhill protein folding. Nature 442(7100):317–321

Saito H, Ando I, Ramamoorthy A (2010) Chemical shift tensor—the heart of NMR: Insights into biological aspects of proteins. Prog Nucl Magn Reson Spectrosc 57(2):181–228

Shen Y, Bax A (2007) Protein backbone chemical shifts predicted from searching a database for torsion angle and sequence homology. J Biomol NMR 38(4):289–302

Shen Y, Lange O, Delaglio F, Rossi P, Aramini JM, Liu G, Eletsky A, Wu Y, Singarapu KK, Lemak A, Ignatchenko A, Arrowsmith CH, Szyperski T, Montelione GT, Baker D, Bax A (2008) Consistent blind protein structure generation from NMR chemical shift data. Proc Natl Acad Sci USA 105(12):4685–4690

Shen Y, Bryan PN, He Y, Orban J, Baker D, Bax A (2009a) De novo structure generation using chemical shifts for proteins with high sequence identity but different folds. Protein Sci 19(2): 349–356

Shen Y, Delaglio F, Cornilescu G, Bax A (2009b) TALOS + : a hybrid method for predicting protein backbone torsion angles from NMR chemical shifts. J Biomol NMR 44(4):213–223

Shen Y, Vernon R, Baker D, Bax A (2009c) De novo protein structure generation from incomplete chemical shift assignments. J Biomol NMR 43(2):63–78

Spronk CAEM, Nabuurs SB, Krieger E, Vriend G, Vuister GW (2004) Validation of protein structures derived by NMR spectroscopy. Progr NMR Spect 45:315–337

Ulmer TS, Ramirez BE, Delaglio F, Bax A (2003) Evaluation of backbone proton positions and dynamics in a small protein by liquid crystal NMR spectroscopy. J Am Chem Soc 125(30): 9179–9191

Varadan R, Walker O, Pickart C, Fushman D (2002) Structural properties of polyubiquitin chains in solution. J Mol Biol 324(4):637–647

Varadan R, Assfalg M, Haririnia A, Raasi S, Pickart C, Fushman D (2004) Solution conformation of Lys63-linked di-ubiquitin chain provides clues to functional diversity of polyubiquitin signaling. J Biol Chem 279(8):7055–7063

Varadan R, Assfalg M, Raasi S, Pickart C, Fushman D (2005) Structural determinants for selective recognition of a Lys48-linked polyubiquitin chain by a UBA domain. Mol Cell 18(6): 687–698

Vasos PR, Hall JB, Kümmerle R, Fushman D (2006) Measurement of 15 N relaxation in deuterated amide groups in proteins using direct nitrogen detection. J Biomol NMR 36(1):27–36

Vila JA, Scheraga HA (2008) Factors affecting the use of 13C(alpha) chemical shifts to determine, refine, and validate protein structures. Proteins 71(2):641–654

Villegas ME, Vila JA, Scheraga HA (2007) Effects of side-chain orientation on the 13C chemical shifts of antiparallel beta-sheet model peptides. J Biomol NMR 37(2):137–146

Wishart DS, Sykes BD, Richards FM (1992) The chemical shift index: a fast and simple method for the assignment of protein secondary structure through NMR spectroscopy. Biochemistry 31(6):1647–1651

Wishart DS, Bigam CG, Yao J, Abildgaard F, Dyson HJ, Oldfield E, Markley JL, Sykes BD (1995) 1H, 13C and 15 N chemical shift referencing in biomolecular NMR. J Biomol NMR 6(2):135–140

Wishart DS, Watson MS, Boyko RF, Sykes BD (1997) Automated 1H and 13C chemical shift prediction using the BioMagResBank. J Biomol NMR 10(4):329–336

Wylie BJ, Sperling LJ, Frericks HL, Shah GJ, Franks WT, Rienstra CM (2007) Chemical-shift anisotropy measurements of amide and carbonyl resonances in a microcrystalline protein with slow magic-angle spinning NMR spectroscopy. J Am Chem Soc 129(17):5318–5319

Wylie BJ, Schwieters CD, Oldfield E, Rienstra CM (2009) Protein structure refinement using 13C alpha chemical shift tensors. J Am Chem Soc 131(3):985–992

Xu XP, Case DA (2001) Automated prediction of 15 N, 13 Calpha, 13 Cbeta and 13 C' chemical shifts in proteins using a density functional database. J Biomol NMR 21(4):321–333

Xu XP, Case DA (2002) Probing multiple effects on 15 N, 13C alpha, 13C beta, and 13C' chemical shifts in peptides using density functional theory. Biopolymers 65(6):408–423

Yao L, Grishaev A, Cornilescu G, Bax A (2010) Site-specific backbone amide (15)N chemical shift anisotropy tensors in a small protein from liquid crystal and cross-correlated relaxation measurements. J Am Chem Soc 132(12):4295–4309

Zhang D, Raasi S, Fushman D (2008) Affinity makes the difference: nonselective interaction of the UBA domain of Ubiquilin-1 with monomeric ubiquitin and polyubiquitin chains. J Mol Biol 377(1):162–180

Zhang D, Chen T, Ziv I, Rosenzweig R, Matiuhin Y, Bronner V, Glickman MH, Fushman D (2009) Together, Rpn10 and Dsk2 Can Serve as a Polyubiquitin Chain-Length Sensor. Mol Cell 36:1018–1033

Zuiderweg ER (2002) Mapping protein-protein interactions in solution by NMR spectroscopy. Biochemistry 41(1):1–7